A stomatal control model based on optimization of carbon gain versus hydraulic risk predicts aspen sapling responses to drought

Martin D. Venturas (ID)**, John S. Sperry, David M. Love** (ID)**, Ethan H. Frehner, Michael G. Allred, Yujie Wang** (ID) **and William R. L. Anderegg**

Department of Biology, University of Utah, 257 S 1400E, Salt Lake City, UT 84112, USA

Summary

- Empirical models of plant drought responses rely on parameters that are difficult to specify *a priori*. We test a trait- and process-based model to predict environmental responses from an optimization of carbon gain vs hydraulic risk.
- We applied four drought treatments to aspen (*Populus tremuloides*) saplings in a research garden. First we tested the optimization algorithm by using predawn xylem pressure as an input. We then tested the full model which calculates root-zone water budget and xylem pressure hourly throughout the growing season.
- The optimization algorithm performed well when run from measured predawn pressures. The per cent mean absolute error (MAE) averaged 27.7% for midday xylem pressure, transpiration, net assimilation, leaf temperature, sapflow, diffusive conductance and soil-canopy hydraulic conductance. Average MAE was 31.2% for the same observations when the full model was run from irrigation and rain data. Saplings that died were projected to exceed 85% loss in soil-canopy hydraulic conductance, whereas surviving plants never reached this threshold.
- The model fit was equivalent to that of an empirical model, but with the advantage that all inputs are specific traits. Prediction is empowered because knowing these traits allows knowing the response to climatic stress.

Introduction

Droughts have dramatic effects on plant communities and can lead to widespread dieback, mortality and productivity loss (e.g. Rice *et al.*, 2004; Allen *et al.*, 2010; Anderegg *et al.*, 2012; Venturas *et al.*, 2016). Climate models predict increased aridification in many regions, with more frequent and severe droughts (IPCC, 2014). How this will affect ecosystems is unclear because we still do not have models that can adequately predict plant responses to drought (Powell *et al.*, 2013). New modeling approaches need to be developed for better drought prediction performance (Smith *et al.*, 2014; Fisher *et al.*, 2018). Models that predict plant hydraulic capacity are particularly useful because mortality risk has been linked to excessive vascular damage (Anderegg *et al.*, 2015; Sperry & Love, 2015; Adams *et al.*, 2017; Rodríguez-Calcerrada *et al.*, 2017; Venturas *et al.*, 2017).

A central challenge to predicting the drought response is modeling how stomata regulate carbon uptake and water use. Stomata adjust to multiple cues (light, CO_2 concentration, water status of soil, plant and atmosphere) via complex stimulus–response mechanisms. Mechanistic models provide insight, but are incomplete and can be difficult to parameterize (Buckley & Mott, 2013). Most canopy-scale models (Tuzet *et al.*, 2003; Powell

et al., 2013; Anderegg *et al.*, 2017; Drake *et al.*, 2017) resort to empirical representations of stomatal conductance (G):

$$G = f(A, C, \text{WS}, c_1, c_2 \ldots c_i) \qquad \text{Eqn 1}$$

where A is the rate of photosynthesis, C is CO_2 concentration either in the leaf or air, WS is a measure of soil or plant water status, and c_1, c_2, etc., are empirically determined coefficients that are usually constant for a particular species or functional type. At each time step, submodels based on photosynthetic biochemistry, diffusion and hydraulics of plant and/or soil provide the array of physiologically possible choices for G, A, C and WS. Iteration chooses the unique G, A, C and WS output that satisfies Eqn 1 for a predetermined set of coefficients. This approach captures responses to light, CO_2 and water status, and provides good fits to a wide range of data sets with numerical economy (e.g. Drake *et al.*, 2017). The problem resides in the coefficients. These fitted parameters are not specific traits or entities that can be measured or estimated *a priori*, so it is ambiguous whether they will apply to novel future conditions. The lack of explicit linkage of these inputs to trait and physiology undermines the predictive power of these models, and obscures an understanding of why

a particular type of vegetation responds differently to environment than another type.

A recent approach eliminates the need for these coefficients by basing the choice of G, A, C and WS on an assumption of how plants balance advantage of greater A vs the concomitant disadvantage of declining WS (Sperry *et al.*, 2017). It has long been recognized that stomatal regulation is potentially constrained by the need to avoid excessive xylem cavitation (Tyree & Sperry, 1988; Jones & Sutherland, 1991; Brodribb *et al.*, 2003). Accordingly, the stomatal 'goal' is to maximize carbon gain while limiting hydraulic risk (Sperry & Love, 2015; Sperry *et al.*, 2016, 2017; Wolf *et al.*, 2016; Anderegg *et al.*, 2018). The 'gain-risk' model of Sperry *et al.* (2017) assumes that stomata maintain a canopy xylem pressure (P_c, a specific measure of WS) that makes the marginal normalized carbon gain ($\delta A'/\delta P_c$) equal to the marginal normalized risk of hydraulic failure ($\delta\theta'/\delta P_c$) at each time step. The values of A' and θ' are scaled from 0 (lowest) to 1 (highest) at each time step (Fig. 1), representing an equal weighting in the trade-off (Wolf *et al.*, 2016; Sperry *et al.*, 2017). A' is calculated from standard models of photosynthesis. The risk, θ', is the fractional loss of the limiting hydraulic conductance at the downstream end of the transpiration stream relative to $\theta' = 0$ for zero transpiration. The risk rises to $\theta' = 1$ at the maximum transpiration rate (E_{crit}) at incipient hydraulic failure and desiccation. The gain-risk model has a minimal set of parameters all of which

are specific traits of plant, soil or environment (Fig. 1). The algorithm predicts the expected responses to changes in environmental conditions such as atmospheric CO_2 concentration, air vapor pressure deficit, air temperature, light intensity and soil moisture (Sperry *et al.*, 2017). Meta-analysis of measured stomatal responses is strongly consistent with the gain-risk optimization (Anderegg *et al.*, 2018). In this paper we test the gain-risk model head-to-head with observations during controlled drought experiments in a research garden setting.

There were two objectives. (1) Test the gain-risk algorithm in isolation by running the Sperry *et al.* model from predawn xylem pressure, thereby avoiding the additional uncertainty of predicting predawn pressure from the root-zone water budget. For comparison, the same was done using Tuzet's empirical model (Tuzet *et al.*, 2003). (2) Test the full gain-risk model, which includes the calculation of the root-zone water budget and predawn pressure at hourly intervals over the growing season from evapotranspiration, irrigation and rain. Model inputs were measured as completely as possible to minimize the impact of parameter error (vs model assumptions). Multiple drought treatments challenged the model with a range of stress and post-stress recovery. Some plants were stressed to death, which allowed us to opportunistically assess whether the model's predictions of vascular dysfunction were consistent with a hydraulic threshold for drought mortality.
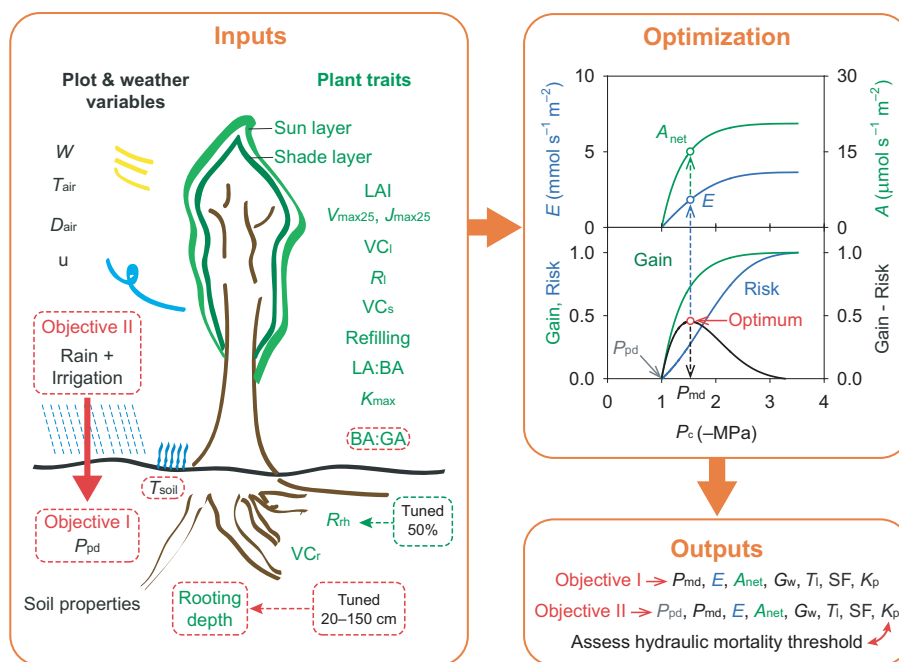

Fig. 1 Model framework. Model inputs include weather, stand and plant traits. The model divides canopy into sun and shade layers which can be run with or without xylem refilling. At each time step, the optimization algorithm finds the canopy pressure (P_c) that maximizes the difference between the gain (A') and risk (θ') functions, yielding outputs. To test the optimization algorithm (Objective I), the predawn xylem pressure (P_{pd}) was an input. To test the full model (Objective II) the root-zone water budget was solved from rain and irrigation, and the model was run for consecutive hourly time steps throughout the growing season. Variables or traits within a broken red line box were exclusively used for Objective II. Input abbreviations: solar radiation (W), air temperature (T_{air}), air vapor pressure deficit (D_{air}), wind speed (u), soil temperature (T_{soil}), predawn pressure (P_{pd}), leaf area index (LAI), maximum carboxylation rate (V_{max25}), maximum electron transport rate (J_{max25}), per cent resistance in the leaf (R_l), leaf vulnerability curve (VC_l), stem vulnerability curve (VC_s), leaf to basal area ratio (LA : BA), maximum plant conductance (K_{max}), basal area to ground area ratio (BA : GA), average per cent resistance in the rhizosphere (R_{rh}) and root vulnerability curve (VC_r). Output abbreviations: midday pressure (P_{md}), transpiration (E), net assimilation (A_{net}), leaf diffusive conductance (G_w), leaf temperature (T_l), sap flow (SF) and whole-plant hydraulic conductance (K_p).

Materials and Methods

Experiments were performed at the University of Utah's Biology Department Growth Facility (Salt Lake City, Utah, USA; 40°45′38.50″N, 111°49′49.94″W at 1494 m). In April 2016 the plot was tilled and planted with 4-yr-old aspen (*Populus tremuloides* Michx.). Saplings were grown from seed (Boundary County, Idaho, USA), and were obtained from High Mountain Nursery (Draper, UT, USA). Roots were rinsed and planted in 0.5 m holes in five 3.2×3.2 m blocks separated by 1.5 m. Each block contained 16 trees in a 0.8×0.8 m square grid, with the model being evaluated on four central ('core') saplings to avoid edge effects (Supporting Information Fig. S1). Sprinklers provided homogenous watering (Fig. S1). Four blocks were assigned different irrigation treatments, and the fifth used for destructive measurements. Saplings were irrigated to field capacity throughout the 2016 growing season. Blocks were weeded regularly.

Drought treatments

From the beginning of the 2017 growing season until day 178 (of 2017), plots were irrigated to field capacity. After that date four treatments were applied: (1) *control*, full irrigation continued throughout the growing season (to day 258); (2) *drought recovery*, limited irrigation during days 179–227 so that plants developed moderate predawn xylem pressure (P_{pd}), and afterwards plants were irrigated to field capacity; (3) *moderate drought*, intermediate P_{pd} sustained throughout the experiment; and (4) *severe drought*, limited irrigation during the whole experiment. The site is on several meters of landfill, and saplings had no groundwater access. The limited summer rainfall at the site was not excluded. Treatment blocks were not replicated because the purpose was not to compare treatments but to induce the full range of drought experience for challenging the model.

Model description

The model was modified from Sperry *et al.* (2017; versions provided in Notes S1–S5). The plant is represented by canopy (all leaves in parallel) and stem (all stems in parallel) elements in series, connected to five root elements in parallel, each connected via in-series rhizosphere elements to bulk soil in five horizontal layers. Layers contained equal root biomass based on

$$M = 1 - B^d \qquad \text{Eqn 2}$$

where M is biomass fraction above depth d (in cm), with inputted B determining the depth profile (maximum depth was d at $M = 0.995$; inputs listed in Table 1 and Fig. 1). Boundary conditions at each timestep are bulk soil water potential (P_s) in each layer, and atmospheric inputs (vapor pressure deficit, D_{air}; solar radiation, W; windspeed, u; air temperature, T_{air}; and soil surface temperature, T_{soil}).

For each time step, transpiration rate (E) is incremented from zero (no cuticular transpiration) to its maximum before hydraulic

failure (E_{crit}). At each E increment the steady-state pressure drop is calculated across each element in the continuum (rhizosphere, root, stem, leaf) using the integral transform method:

$$E = \int_{P_{up}}^{P_{down}} K(P)\,\mathrm{dp} \qquad \text{Eqn 3}$$

$P_{up} - P_{down}$ is the pressure drop across the element, and $K(P)$ is the unsaturated conductivity function for the rhizosphere (van Genuchten functions were used; Table 1) or xylem element vulnerability curves (root, VC_r; stem, VC_s; leaf, VC_l). Vulnerability to cavitation curves were represented by a two-parameter Weibull function:

$$K = K_{max} \cdot e^{-\left(\frac{p}{b}\right)^c} \qquad \text{Eqn 4}$$

where K is hydraulic conductance of the element, K_{max} the element's maximum without cavitation, and b and c are curve parameters. Incrementing E yields its steady-state relationship with canopy pressure, P_c (Fig. 1; the supply function of Sperry & Love (2015) and Sperry *et al.* (2017)). Fluxes and conductances were scaled from leaf- to basal- to ground-area using leaf area per basal area (LA : BA) and basal area per ground area (BA : GA).

The derivative of the E vs P_c supply function is proportional to the hydraulic conductance of the downstream end of the flow-path ($K_c = \mathrm{d}E/\mathrm{d}P_c$), which falls from a maximum (K_{cmax}) at $E = 0$ to near zero at $E = E_{crit}$ when the plant has no functional xylem. The risk function is the fractional loss of K_c:

$$\theta' = 1 - \frac{K_c}{K_{cmax}}, \qquad \text{Eqn 5}$$

and it rises from 0 at $E = 0$ to 1 at $E = E_{crit}$ (Fig. 1).

For the same time step the model calculates net photosynthesis (A_{net}) from each E increment (Fig. 1) in the following sequence: (1) leaf temperature (T_l) is obtained from E, W and leaf width (L_w) via leaf energy budget; (2) leaf-air vapor pressure deficit (D_l) is calculated from T_l and D_{air}; (3) diffusive conductance to water vapor (G_w, boundary + stomatal components) is given by $G_w = E/D_l$; (4) diffusive conductance to CO_2, G_c, is estimated as $G_c = G_w/1.6$ (diffusive transport assumed); and (5) A_{net} is calculated from a Farquhar-type model as implemented by Medlyn *et al.* (2002) and detailed in Sperry *et al.* (2017). Inputs include the maximum rates of carboxylation (V_{max25}) and electron transport (J_{max25}) at 25°C. Leaf respiration at 25°C was set to $V_{max25} \times 0.01$ (Collatz *et al.*, 1991). A_{net} is converted to a normalized gain function:

$$A' = \frac{A_{net}}{A_{max}} \qquad \text{Eqn 6}$$

where A_{max} is the maximum A_{net} at that time step, which is usually at E_{crit}. The model finds the maximum gain–risk difference with respect to P_c (Fig. 1):

Table 1 Major model inputs and outputs with their abbreviation, definition and units

Abbreviation	Definition	Units
Inputs		
BA : GA	Plant basal area to ground area ratio[b]	$m^2\,m^{-2}$
d	Maximum rooting depth[b]	cm
D_{air}	Atmospheric vapor pressure deficit	kPa
H	Plant height	m
Irrigation	Water input due to irrigation[b]	mm
J_{max25}	Maximum electron transport rate at 25°C	$\mu mol\,m^{-2}\,s^{-1}$
K_{max}	Maximum whole-plant conductance	$kg\,h^{-1}\,MPa^{-1}\,m^{-2}$
LA : BA	Leaf area to basal area ratio	$m^2\,m^{-2}$
LAI	Leaf area index	$m^2\,m^{-2}$
L_w	Leaf width	m
P_{pd}	Predawn xylem pressure[a]	MPa
Rain	Water input due to rain[b]	mm
R_l	Initial per cent resistance to flow in the leaf	%
R_{rh}	Per cent resistance to flow in the rhizosphere	%
Soil properties	van Genuchten parameters n and α (MPa^{-1}); field capacity[b] ($m^3\,m^{-3}$)	
T_{air}	Air temperature	°C
T_{soil}	Soil temperature[b]	°C
u	Wind speed	$m\,s^{-1}$
VC_l	Leaf vulnerability curve (Weibull curve b and c parameters)	
VC_r	Root vulnerability curve (Weibull curve b and c parameters)	
VC_s	Stem vulnerability curve (Weibull curve b and c parameters)	
V_{max25}	Maximum carboxylation rate at 25°C	$\mu mol\,m^{-2}\,s^{-1}$
W	Solar radiation	$W\,m^{-2}$
Outputs		
A_{net}	Net photosynthesis assimilation per unit of leaf area	$\mu mol\,CO_2\,s^{-1}\,m^{-2}$
E	Transpiration per unit of leaf area	$mmol\,H_2O\,s^{-1}\,m^{-2}$
G_w	Canopy diffusive conductance (stomatal plus boundary layer)	$mmol\,H_2O\,s^{-1}\,m^{-2}$
K_p	Whole-plant conductance per basal area	$kg\,h^{-1}\,MPa^{-1}\,m^{-2}$
K_x	Xylary pathway conductance per basal area	$kg\,h^{-1}\,MPa^{-1}\,m^{-2}$
P_{md}	Midday canopy xylem pressure	MPa
P_{pd}	Predawn xylem pressure[b]	MPa
P_s	Soil water pressure[b]	MPa
PLC_p	Whole-plant per cent loss in conductance	%
PLC_x	Whole-plant xylem per cent loss in conductance	%
SF	Whole-plant sap flow per basal area	$kg\,h^{-1}\,m^{-2}$
T_l	Leaf temperature	°C

[a]Only for Objective I.
[b]Only for Objective II.

$$A' - \theta' = \text{maximum} \qquad \text{Eqn 7}$$

which yields the outputs for that time step: P_c, E, A_{net}, G_w, T_l, SF (tree sapflow per basal area) and K_p (soil-canopy hydraulic conductance per basal area). Separate gain functions are computed for sun and shade layers (Fig. 1) of the canopy following the light model of Campbell & Norman (1998; Methods S1) which requires canopy leaf area index (LAI). When photosynthetic photon flux density is below $30\,\mu mol\,s^{-1}\,m^{-2}$, the stomata remain closed. Sun-layer and whole-tree outputs were evaluated.

With xylem refilling turned on, $K(P)$ functions have no hysteresis. With refilling turned off, the model assumes no effect of prior drought on P_c, but fluxes and conductances are reduced according to a permanent loss of *xylem* hydraulic conductance caused by the most negative prior pressure (rhizosphere conductance recovers). This behavior is consistent with observed

post-drought recovery (Brodribb & Cochard, 2009; Resco *et al.*, 2009; Brodribb *et al.*, 2010).

Objective I

To test the gain–risk algorithm, bulk soil P_s was inputted for each time step as the measured P_{pd} (minus the gravity gradient from sapling height) from the core saplings (Notes S2, S3). Atmospheric boundary conditions were midday values (11:00–12:00 h Mountain Standard Time, MST), and the gain–risk algorithm predicted midday outputs. The sequence of time steps corresponded to 16 evenly spaced 'measurement days' when P_{pd} and midday model outputs were assessed. Predictions were made on a per tree basis because P_{pd} could differ between core trees within drought treatments. Treatments were pooled to compare model predictions vs measurements.

All model inputs were measured (below) except for the K_{max} of the rhizosphere (required for the van Genuchten $K(P)$ function

of the rhizosphere element), which depends on rhizosphere thickness and root surface area. Rhizosphere K_{max} is set by designating a mean percentage rhizosphere resistance (R_{rh}; percentage of total soil-canopy resistance), which is averaged over the full P_s range from 0 to P_{crit} (i.e. P_c at E_{crit}). We chose the R_{rh} setting that minimized MAE between studentized predictions and measurements for P_c, E, A_{net}, T_l, G_w and SF across treatments. Studentized values (predicted and measured) were obtained by subtracting the measured mean and dividing by the measured standard deviation, hence normalizing for equal MAE weighting.

Uncertainty of model predictions was estimated by bootstrapping mean inputs 1000 times for each tree, yielding 4000 model predictions per treatment from which the 95% confidence intervals were estimated. Bootstrapping sampled with replacement except in a few cases (see measurement of model inputs). The model prediction of treatment P_c, E, A_{net}, T_l, G_w, SF and K_p was evaluated in three ways: (1) overlapping of 95% confidence intervals (CIs) between prediction and measurement, (2) MAE reported in absolute value, and as a percentage of the measured mean, and (3) the measured vs modeled r^2. The model was tested with and without xylem refilling.

The importance of 16 major inputs on the variance of model outputs (no refilling) was assessed with a Sobol global sensitivity analysis (Nossent *et al.*, 2011). Inputs were varied (independently, except for pairing of Weibull b and c, and V_{max25} and J_{max25}) across a specified range, and each input's portion of each output's variance was estimated. Variance due to a direct effect of the input as well as the total effect (including interactions with other inputs) was calculated. Plant inputs were varied across their bootstrapped range, except for R_{rh} which was varied from 45% to 55% (centered on the 50% estimate, see Results). Weather inputs were varied across the 16-d observed range. Two P_{pd} inputs were tested, the first (P_{pd1}) representing exposure to prior drought and the second (P_{pd2}) the current value. For each input, the variance portion was estimated from 4000 output values.

For comparison with the prevailing empirical approach we chose Tuzet's model (Tuzet *et al.*, 2003) because it also uses P_c as the measure of plant water status. Tuzet's model as applied by Drake *et al.* (2017) satisfies the equality:

$$G_c = G_0 + \frac{c_1 \cdot A_{net} \cdot \left(1 + e^{(c_2 \cdot P_{ref})}\right)}{C_a \cdot \left(1 + e^{(c_2 \cdot (P_{ref} - P_c))}\right)} \qquad \text{Eqn 8}$$

where G_0 is the 'residual conductance' to CO_2, c_1 and c_2 are empirical coefficients, P_{ref} is a 'reference' leaf xylem pressure (an empirical factor), and C_a is ambient CO_2 concentration. We set G_0 to zero because zero cuticular conductance was assumed in the gain–risk model. We obtained c_1 (4.82), c_2 (0.46) and P_{ref} (0 MPa) by minimizing the MAE between calculated vs measured G_c, A_{net} and P_c (values studentized for equal weighting) across all trees and treatments. P_{ref} was constrained to be zero or negative. For each measured P_{pd} we iteratively solved Eqn 8 with the photosynthetic and hydraulic routines used to generate the gain and risk curves, assuming no xylem refilling (Methods S2; Notes S4).

Objective II

The full model (no refilling) was run for hourly time steps from day 171 to day 258, starting from soil at field capacity (Notes S5). After each time step, bulk soil water content and P_s boundary conditions were re-calculated for each soil layer. Net flow into each layer during the previous time step was added to the layer's old volumetric water content to obtain the new water content and soil P_s for the next time step. Net flow was the sum of four components. (1) Flow across the rhizosphere, which was calculated along with the E vs P_c supply function. When E is low or zero, the model gives the hydraulic redistribution from wet to dry layers. (2) Rain or irrigation during the previous time step, which was assumed to instantly infiltrate the soil to field capacity from the top down with no runoff or interception. (3) Soil evaporation from a rootless 2-cm surface layer was modeled by reducing its potential evaporation rate (at field capacity) in rough proportion to the relative humidity at the soil surface (Eqn 9.14 of Campbell, 1985). The potential evaporation rate was estimated from soil surface energy budget simplified by the measurement of T_{soil} (Campbell & Norman, 1998; Methods S1). (4) Redistribution between layers via soil was estimated from the integral transform of the van Genuchten $K(P_s)$ function (scaled for vertical distance between layer mid-points) over the difference in layer P_s.

Measured inputs were the same as for objective I, except that P_{pd} was an output. Plant inputs that varied across the 16 measurement days (e.g. V_{max25} and J_{max25}, BA : GA, plant height, LAI) were interpolated between measurements. Soil field capacity was calibrated to minimize the MAE of predicted vs measured control P_{pd} for the 16 measurement days. Rooting depth had no effect on control output, but influenced drought treatment output. Maximum root depth for each core sapling was estimated as the value minimizing the P_{pd} MAE over the 16 measurement days.

The full model was evaluated in the same way as for objective I for the 16 measurement days. Bootstrapping was not feasible owing to computation time. The model's hourly SF output was compared with hourly SF measurements.

Mortality threshold analysis

Logistic probability regression (Menard, 2002) quantified the relationship between modeled minimum seasonal hydraulic conductance in surviving saplings vs saplings that died. Mortality was judged by failure of saplings to recover by spring 2018, and it was associated with complete canopy desiccation during the 2017 experiment. Minimum soil-canopy hydraulic conductance was assessed as absolute minimum K_p or maximum percentage loss relative to pre-drought K_p (PLC_p). Conductance was also assessed for the plant's xylem flow path (K_x and PLC_x). Minimum conductance in dying saplings was determined until the first observance of total canopy desiccation and also as if the desiccated saplings had survived the entire season.

Measurement of model inputs

Hourly precipitation, T_{air}, D_{air}, T_{soil}, W and u were averaged from values registered every 10 min at an onsite station (iUTAH GAMUT network, station RG_GRF_C, iutahepscor.org). Irrigation was measured with a flow meter (model FTB8007B-PT, Omega, Stamford, CT, USA) connected to a datalogger (CR-10X; Campbell Scientific, Logan, UT, USA). Treatments were watered at 19:45–21:00 h MST to minimize evaporation and to allow infiltration before P_{pd} measurements.

The van Genuchten soil parameters (n and α) and saturated water content were determined from soil texture. Two soil samples were taken from each treatment block (0–30 and 30–60 cm depth) and sent to the Utah State University Analytical Laboratory (Logan, UT, USA). Water content was adjusted for measured fraction of rocks in the soil (Methods S3).

Plant height (H, required to compute gravity gradient in P) and BA : GA for the core saplings were measured at the beginning (day 171), middle (day 220), and end (day 269) of the experiment. The LA : BA and L_w were measured on six saplings from the extra block at the beginning of the experiment (leaf area meter Li3100; Li-Cor, Lincoln, NE, USA). Leaf counts were made on one branch per core tree every 2 wk to estimate the change in LA : BA. LAI was evaluated weekly from four hemispheric pictures per block (Sigma 8 mm EX fisheye lens and Canon 5D camera; Gap Light Analyzer software; Frazer et al., 1999).

The plant $K(P)$ functions required K_{max} for root, stem and leaf elements. These were calculated from soil-canopy K_{max} (the 'saturated' value at $P = 0$), which was calculated from measured K_p on day 178 immediately before imposing treatments. K_p was obtained from midday sapflow (11:00–13:00 h MST; see below) divided by P_{md}–P_{pd}. K_p was bootstrapped by sampling sapflow data with replacement (measured every 10 min), with ± 0.05 MPa accuracy for xylem pressure. The model determined the soil-canopy K_{max} at $P = 0$ that yielded the measured K_p. The K_{max} of the leaves in parallel was estimated from the percentage of well-watered whole-plant resistance ($1/K_p$) that was in the leaves (R_l). R_l was estimated as the average percentage of soil-to-canopy pressure drop (P_{md}–P_{pd}) in the leaves. The leaf pressure drop was the difference between P_{md} of transpiring leaves and P_{md} of non-transpiring leaves covered with adhesive tin foil at predawn. R_l (mean of $n = 6$) was used by the model to set the initial percentage leaf resistance (and hence leaf K_{max}) from whole-plant K_{max}. The remaining K_{max} (after leaf K_{max} was factored out from plant K_{max}) was partitioned 1/3 into the root system and 2/3 in the stem.

The plant $K(P)$ functions required Weibull b and c inputs (Eqn 3). Root ($n = 20$ segments) and stem ($n = 15$) vulnerability curves were constructed using the centrifuge method (Alder et al., 1997) on samples from the extra plot at the beginning of June and again at the end of August. The b and c parameters were obtained from a Weibull curve fit to the pooled data. For bootstrapping, segments were sampled with replacement before obtaining paired b and c values. VC_l was constructed at the end of August from branches collected at native pressures or bench-

top dehydrated. Leaf margins were trimmed to expose minor veins, minimizing extra-xylary flow and promoting the measurement of xylem conductance. Conductance of the whole shoot (stems + leaves) was measured using the vacuum method (Kolb et al., 1996). Stem conductance was similarly measured after removing leaves. Leaf resistance (on a basal area basis) was obtained by subtraction (shoot resistance – stem resistance). A Weibull curve fit yielded b and c parameters. To bootstrap the leaf curve, we sampled leaf conductance data with replacement over modest, moderate and large negative pressure ranges to represent pressure-independent variation.

V_{max25} and J_{max25} were obtained from A–Ci curves (Licor-6400XT with the 3×2 LED chamber, Li-Cor, Lincoln, NE, USA; Methods S4), measured once for each core sapling at the beginning of the experiment (days 172–179), for controls at the middle of the experiment (day 220), and for control and drought-recovery saplings near the end of the experiment (days 238–239). We used the mean V_{max25} and J_{max25} across all measured saplings for each period and interpolated between measurement days. To bootstrap, V_{max25} and J_{max25} pairs (from single A-Ci curves) were sampled with replacement.

Measurement of model output variables

On the 16 measurement days, P_{pd} (04:00 h–06:00 h MST) and midday (11:00 h–12:00 h MST) pressure (P_{md}) were measured on one leaf per core sapling using a pressure chamber (PMS Instruments, Corvallis, OR, USA; precision ± 0.05 MPa). On 13 of these days, midday (10:00 h –13:00 h MST) A_{net}, E, and G_w were also measured on three leaves per core sapling (LiCor-6400XT). Chamber D_{air}, T_{air} and PAR were kept within 10% ambient; $[CO_2]$ was 400 ppm. Leaf temperature was monitored every 10 min using copper-constantan thermocouples on one leaf per core tree.

Energy balance sapflow sensors (Baker & van Bavel, 1987) were installed 2 wk before the drought treatments on the main stem of the 4 core saplings in each treatment (Fig. S1). Measurements were registered every 10 min on a datalogger (CR7; Campbell Scientific, Logan, UT, USA). Sapflow per basal area was calculated from Sakuratani (1981). Outliers were filtered by binning 10-min measurements during hourly timesteps on all four saplings per treatment, and employing Tukey's fence method (Tukey's 'fences'; Tukey, 1977).

Data availability

Data are available in Supporting Information Table S1.

Results

Treatments

Treatments induced different water stress (Fig. 2). The mean P_{pd} for control saplings remained above -0.5 MPa (Fig. 2a), and drought recovery P_{pd} fell to c. -1.2 MPa before rewatering (Fig. 2b). No saplings died in either treatment. The moderate
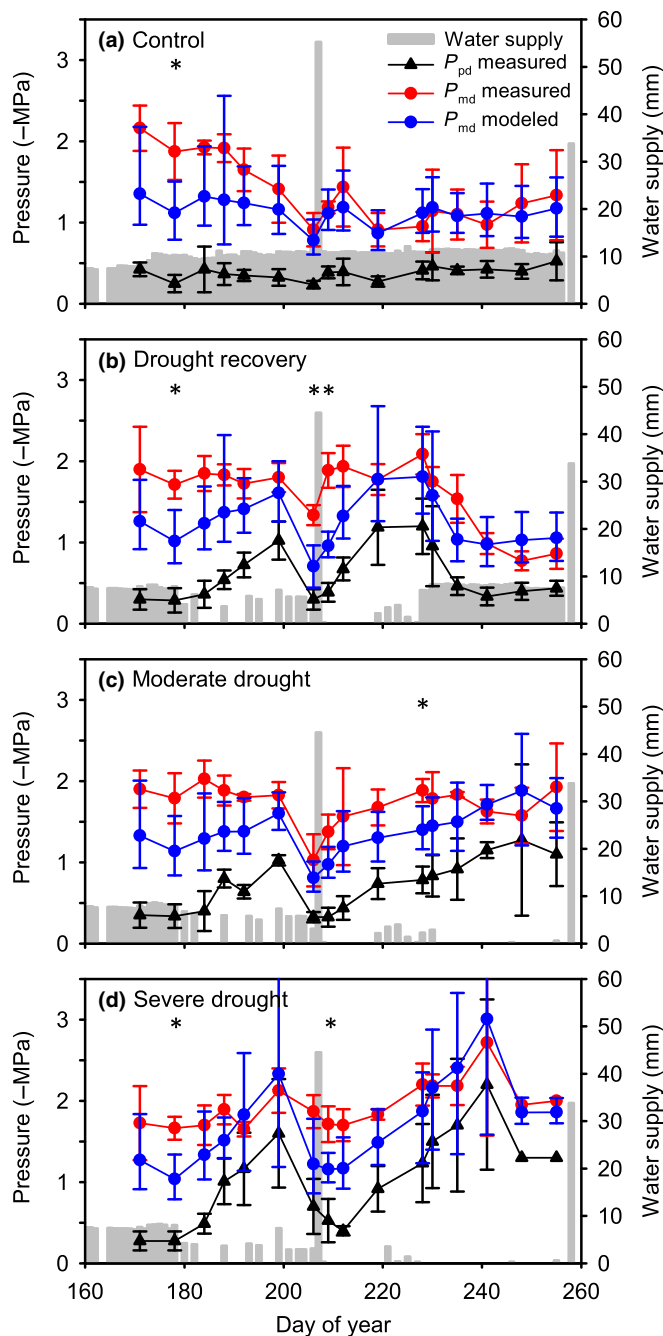
Fig. 2 Model performance for predicting aspen midday pressures (P_{md}) from measured predawn pressures (P_{pd}). Gray bars indicate the total water input (irrigation plus rain) for each treatment: (a) control, (b) drought recovery, (c) moderate drought and (d) severe drought. Mean values from the four core trees per treatment and their 95% CIs are represented (measured P_{pd}, black triangles; measured P_{md}, red circles; modeled P_{md}, blue circles). Asterisks indicate the days when there is no overlap between 95% CIs of measured and modeled P_{md}.

Table 2 Input trait results and information on how each trait was varied for running the model

Trait[a]	Mean ($\pm$ SD)[a]	Varied per
BA : GA	Initial = 2.75×10^{-4} ($\pm 1.01 \times 10^{-4}$)	Sapling
	Final = 3.81×10^{-4} ($\pm 1.43 \times 10^{-4}$)	Time step
d	65.3 (± 37.7)	Sapling
H	Initial = 1.22 (± 0.26)	Sapling
	Final = 1.42 (± 0.27)	Time step
J_{max25}	Initial = 165.0 (± 32.5)	Time step
	Final = 113.0 (± 58.1)	
K_{max}	975.5 (± 202.7)	Sapling
LA : BA	1183.6 (± 278.6)	Constant
LAI	Control: Initial = 0.36 (± 0.02);	Treatment
	Final = 0.36 (± 0.03)	
	Drought recovery: Initial = 0.28 (± 0.03);	Time step
	Final = 0.21 (± 0.02)	
	Moderate drought: Initial = 0.19 (± 0.03);	
	Final = 0.05 (± 0.01)	
	Severe drought: Initial = 0.24 (± 0.04);	
	Final = 0.03 (± 0.01)	
L_w	0.04 (± 0.01)	Constant
R_l	86.0 (± 10.2)	Constant
R_{rh}	No refilling = 50	Constant
	With refilling = 55	
Soil properties	$n = 1.23$	Constant
	$\alpha = 275.5$	
	Saturated water content = 0.38	
	Field capacity fraction = 0.22	
VC_l	$b = 1.71$	Constant
	$c = 1.08$	
VC_r	$b = 1.15$	Constant
	$c = 1.07$	
VC_s	$b = 3.12$	Constant
	$c = 2.64$	
V_{max25}	Initial = 121.8 (± 18.8)	Time step
	Final = 56.8 (± 37.5)	

[a]Abbreviation definitions and units are provided in Table 1.

range of T_{air} (9–37°C), T_{soil} (9–25°C), D_{air} (0–5.6 kPa), W (0–1000 W m^{-2}), and u (0–5 m s^{-1}; Figs S2, S3). One summer storm rehydrated all drought treatments on day 207 (Fig. 2).

Traits

Soil was sandy clay loam (Table 2) with an average of 7% rock volume. There were no differences in H and BA between treatments. By the end of the experiment, saplings had grown a mean of 0.2 m in H and 0.68 cm^2 in BA. Control LAI showed no trend but LAI of the three drought treatments decreased during the experiment (Table 2). Leaf count per branch, however, remained relatively constant in all treatments, only dropping a few days before a tree's death. Thus, the decline in plot-level LAI resulted from abrupt loss of canopy in dying trees, rather than from gradual leaf shedding across all trees. Hence, modeling assumed a constant LA:BA.

There was no difference between the VC_r and VC_s measured at the beginning of July and the end of August, and the data were pooled. Pressure at which 50% loss in conductivity was reached (P_{50}) indicated that roots ($P_{50} = -0.82$ MPa) and leaves ($P_{50} = -1.22$ MPa) were more vulnerable to cavitation than
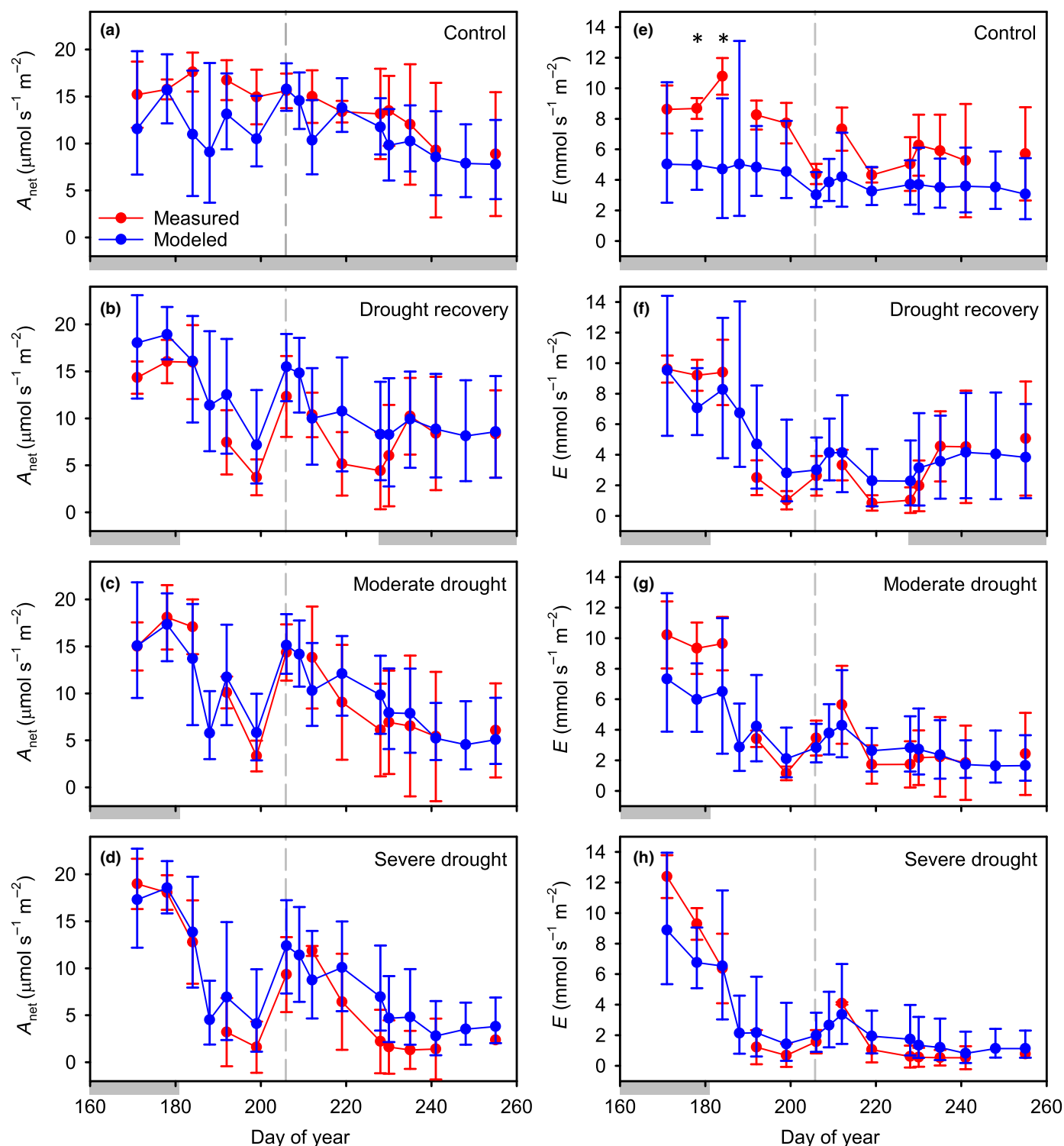
drought P_{pd} dropped to -1.3 MPa on average, and severe drought reached -2.2 MPa (Fig. 2c,d). Moderate drought desiccated the canopies of 2 of the 4 core saplings, and severe drought desiccated 3 core saplings (additional edge trees also desiccated in both treatments). Desiccated saplings died based on lack of recovery by the following spring. Saplings experienced a wide

Fig. 3 Model performance for predicting aspen net assimilation (A_{net}) and transpiration (E) from observed predawn pressures (P_{pd}). (a–d) Mean measured (red circles) and modeled (blue circles) net assimilation and (e–h) transpiration for each treatment with their 95% CIs. Gray rectangles by the x-axis represent the period during which plants were watered to field capacity (see Fig. 2 for water inputs). The vertical gray dashed line was a large rainstorm. Asterisks indicate days when there was no overlap between 95% CIs.

stems ($P_{50} = -2.72$ MPa; Table 2). The R_l averaged 86% in well watered plants (Table 2) and fell considerably to 44% in droughted plants.

Photosynthetic capacity (V_{max25} and J_{max25}) of leaves dropped during the experiment (Table 2). This drop was equal for control and drought recovery treatments (the only treatments for which
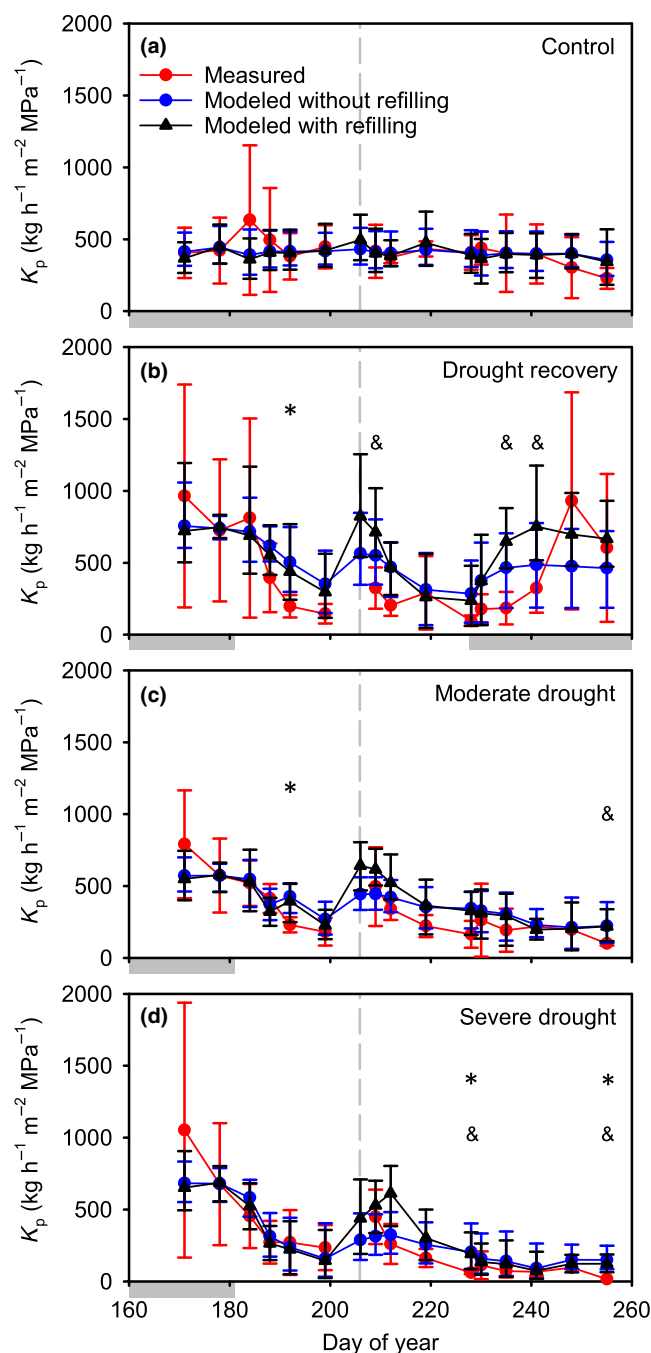
Fig. 4 Comparison between measured and modeled aspen whole-plant conductance (K_p) with and without refilling. Measured (red circles), modeled without refilling (blue circles) and modeled with refilling (black triangles) means and 95% CIs for (a) control, (b) drought recovery, (c) moderate drought and (d) severe drought treatments. Asterisks denote no overlap in 95% CI between measured and modeled without refilling, and symbols denote the same for the refilling model. Gray rectangles by the x-axis show when plants were watered to field capacity. The vertical gray dashed line indicates a large rainstorm (see Fig. 2 for water inputs).

Table 3 Performance of the model for predicting the mean treatment values run in three different modes and performance of the Tuzet model

Variable[a]	Units	95% CI overlaps (%)	MAE (absolute)[b]	MAE (%)[b]	r^2
Objective I. Without refilling					
A_{net}	µmol m^{-2} s^{-1}	100.0	2.3	22.8	0.72
E	mmol m^{-2} s^{-1}	96.2	1.6	33.9	0.79
G_w	mmol m^{-2} s^{-1}	94.2	59.9	41.1	0.60
K_p	kg h^{-1} m^{-2} MPa^{-1}	93.3	108.1	29.9	0.64
P_{md}	MPa	89.1	0.4	21.4	0.50
SF	kg h^{-1} m^{-2}	100.0	151.2	39.4	0.82
T_l	°C	73.3	1.7	5.2	0.80
Average		92.3		27.7	0.69
Tuzet model. Without refilling					
A_{net}	µmol m^{-2} s^{-1}		3.5	34.6	0.71
E	mmol m^{-2} s^{-1}		1.4	30.3	0.82
G_w	mmol m^{-2} s^{-1}		51.7	35.5	0.63
K_p	kg h^{-1} m^{-2} MPa^{-1}	93.6		25.9	0.66
P_{md}	MPa		0.4	26.1	0.49
SF	kg h^{-1} m^{-2}		154.5	40.2	0.83
T_l	°C		2.3	7.1	0.79
Average				28.5	0.70
Objective I. With refilling					
A_{net}	µmol m^{-2} s^{-1}	100.0	2.4	23.5	0.70
E	mmol m^{-2} s^{-1}	96.2	1.6	34.1	0.73
G_w	mmol m^{-2} s^{-1}	94.2	57.3	39.4	0.51
K_p	kg h^{-1} m^{-2} MPa^{-1}	90.0	116.7	32.2	0.54
P_{md}	MPa	84.4	0.4	22.5	0.48
SF	kg h^{-1} m^{-2}	100.0	153.8	40.0	0.72
T_l	°C	78.3	1.7	5.2	0.81
Average		91.9		28.1	0.64
Objective II. Without refilling					
A_{net}	µmol m^{-2} s^{-1}		2.6	25.6	0.65
E	mmol m^{-2} s^{-1}		1.9	41.0	0.75
G_w	mmol m^{-2} s^{-1}		69.3	47.6	0.57
K_p	kg h^{-1} m^{-2} MPa^{-1}		107.8	29.8	0.56
P_{md}	MPa		0.4	25.7	0.34
P_{pd}	MPa		0.2	26.1	0.67
SF	kg h^{-1} m^{-2}		169.8	44.2	0.76
T_l	°C		1.5	4.8	0.80
Average[c]				31.2	0.63

[a]Variable definitions are provided in Table 1.
[b]MAE, mean absolute error.
[c]Average excludes P_{pd} from the calculation so that Objectives I and II can be directly compared.

we could construct A–Ci curves at the end of the season), and thus we used the same V_{max25} and J_{max25} (interpolating for different measurement days) for all treatments.

Objective I: testing the gain–risk algorithm

The best fit was obtained with refilling turned off and R_{rh} tuned to 50% (average MAE = 27.7%; Table 3), but similar results were obtained with refilling turned on and R_{rh} = 55% (average MAE = 28.1%). Hereafter we report the results from running the model without refilling unless specified.

The 95% CIs of measured and modeled P_{md}, A_{net}, E, G_w, T_l, K_p and SF overlapped for 92.3% of the 412 comparisons (all variables, days, and treatments; Figs 2,3,4; Table 3). The relative MAE for these variables averaged 27.7% (5.2–41.1%), and r^2 averaged 0.69 (0.50–0.82; Table 3; Fig. 5a). When the 95% CIs failed to overlap, the gain–risk model tended to under-estimate
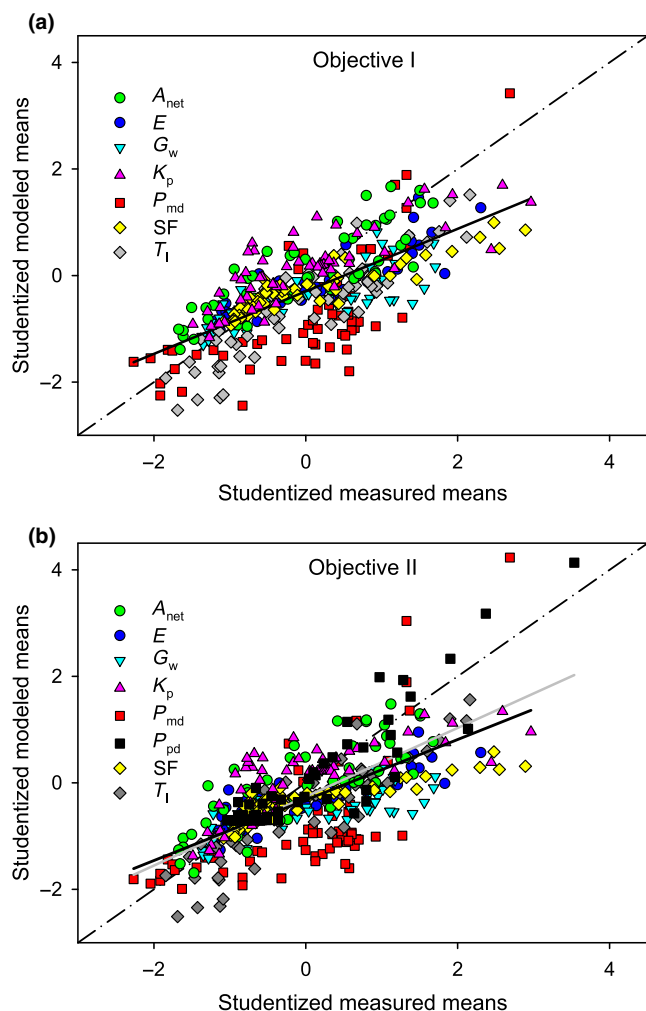
Fig. 5 Studentized measured vs modeled treatment means of the main output variables for aspen. (a) Net assimilation (A_{net}), transpiration (E), diffusive stomatal conductance (G_w), whole-plant hydraulic conductance (K_p), canopy pressure at midday (P_{md}), leaf temperature (T_l) and sap flow (SF) obtained from running the model from measured pressures at predawn (P_{pd}; Objective I). Solid black line is the overall regression for the six outputs ($n = 400$, $P < 0.001$, $r^2 = 0.53$). (b) Same six outputs as in (a) plus P_{pd} obtained from running the full model with soil water budget (Objective II). Solid gray line is the overall regression for the seven variables ($n = 464$, $P < 0.001$, $r^2 = 0.43$), and the solid black line is the overall regression for the six variables of (a) (i.e. excluding P_{pd}, $n = 400$, $P < 0.001$, $r^2 = 0.41$). Dash–dot lines represent the 1 : 1 relationship.

P_{md} and E (Figs 2, 3). The model performed better at predicting A_{net} (Fig. 3a–d) and E (Fig. 3e–h), than G_w and SF (Table 3; Fig. 5a). Considering all outputs together, the model had a flatter response to environmental stimuli than the measurements (Fig. 5a). Tuzet's model had a similar overall MAE, averaging 28.5% vs 27.7% as well as similar average r^2 of 0.70 vs 0.69 (Table 3). Midday pressures were more negative than observed, but Tuzet estimates overall were more centered on the 1 : 1 relationship (Figs S4 vs 5a).

The small difference between running the gain–risk model with and without refilling (Table 3) was consistent with the fact that measured K_p showed intermediate recovery (Fig. 4). This

was most evident in the drought recovery treatment where measured K_p remained depressed for several days after rewatering (Fig. 4b) before eventually rising back to near initial values. The no-refilling model under-predicted this recovery, whilst it was over-predicted by the refilling model. Similarly equivocal patterns were observed after the single major rain event on day 207 (Fig. 4, vertical dashed gray line). Measured K_p increased after this rain, but rarely to initial values. This response was bracketed by the model output: no-refilling predicted modest post-rain recovery owing to recovering rhizosphere hydraulic conductance, and refilling predicted full recovery.

According to the Sobol analysis, variance in the P_{md} output was overwhelmingly attributed to the current P_{pd} (P_{pd2}, Fig. 6a), with much smaller effects of V_{max25} (and its J_{max25} pair), vulnerability curves, plant K_{max} and D_{air}. The current P_{pd} was also the biggest contributor to variance in fluxes (SF, E, A_{net}) and G_w, but other important influences included prior drought exposure (P_{pd1}; no refilling), the leaf vulnerability curve and plant K_{max} (Fig. 6b–d, f). Variance in A_{net} was also importantly influenced by V_{max25} (and its paired J_{max25}) and D_{air} (Fig. 6f). The T_l variance was overwhelmingly determined by T_{air}, with minor influences of W and D_{air} (Fig. 6e). Overall, A_{net} variance was sensitive to the most inputs (Fig. 6f).

Objective II: testing the full model

A soil field capacity calibration of 0.084 m^3 m^{-3} achieved a minimum MAE of 0.058 MPa for measured vs modeled P_{pd} in control trees over the 16 measurement days. The best-fit rooting depth in droughted trees averaged 0.69 m (range 0.20–1.50 m), yielding an MAE of 0.15 MPa between measured and modeled P_{pd}. Across all treatments, the full model predicted P_{pd} with an MAE of 0.18 MPa (26.1%) and an r^2 of 0.67 (Table 3; Fig. 5b). For comparison, if we assumed a field capacity of half the saturated capacity (0.19 m^3 m^{-3}; Campbell, 1985), the MAE for P_{pd} was 0.38 MPa (56.1%), yielding an overall MAE = 34.0% and $r^2 = 0.60$ for the same seven variables. Estimated rooting depth was shallower, averaging 0.27 m (range 0.10–0.55 m).

The additional uncertainty of modeling the root-zone water budget only slightly increased model error for the same set of 16 midday observations tested in Objective I (Fig. 5b; Table 3). The overall MAE for P_{md}, A_{net}, E, G_w, T_l, SF and K_p across the 16 d and four treatments increased only 3.5% (from 27.7% to 31.2%). The average r^2 decreased from 0.69 to 0.63 (range 0.34–0.80; Fig. 5).

Moving from midday to hourly scale, the error in predicting SF increased from 44.2% to 45.0%, and r^2 decreased from 0.76 to 0.70 (Table 3 vs Fig. 7b). The model predicted a smaller SF range than was observed (Fig. 7b) chiefly because it underestimated the very high sapflow rates early in the season (Fig. 7a).

Mortality thresholds

The PLC$_p$ values cycled diurnally with E because of the reversible hydraulic resistance in the rhizosphere (Fig. 8a); the permanent PLC$_p$ increase resulted from irreversible xylem cavitation. No

Fig. 6 Sobol sensitivity analysis for testing the optimization algorithm (Objective I). Direct effects (hatched) and total effects (hatched+gray) of 16 major inputs (*x* axis) on aspen outputs: (a) pressure at midday, P_{md}, (b) sap flow, SF, (c) transpiration, *E*, (d) stomatal diffusive conductance, G_w, (e) leaf temperature, T_l, and (f) net assimilation, A_{net}. Input abbreviations: K_{max}, maximum soil-canopy hydraulic conductance; VC_r, root vulnerability curve; VC_s, stem vulnerability curve; VC_l, leaf vulnerability curve; R_{rh}, average per cent resistance in rhizosphere; R_l, per cent resistance in leaf; LA : BA, leaf area per basal area; L_w, leaf width, V_{max25}, maximum carboxylation rate (coupled to maximum electron transport rate, J_{max25}); P_{pd1}, minimum prior predawn xylem pressure experienced; P_{pd2}, current predawn xylem pressure; *W*, solar radiation; T_{air}, air temperature; *u*, wind speed, D_{air} air vapor pressure deficit; LAI, leaf area index.
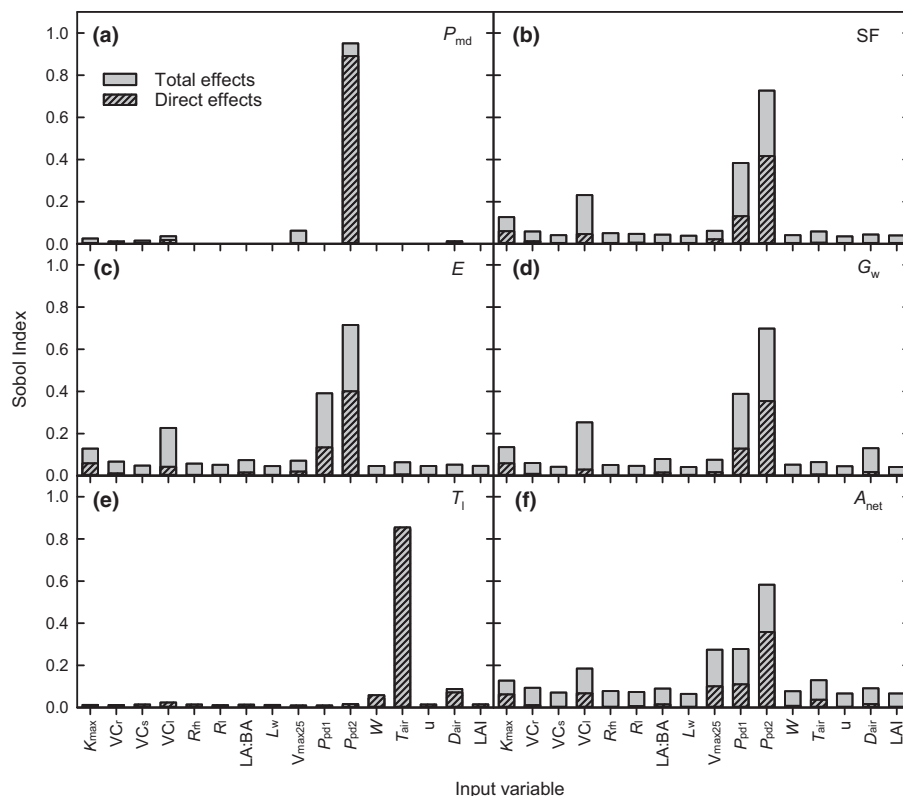
sapling reached 100 PLC_p. All five saplings that died were projected to exceed 84.9 PLC_p by the end of the growing season, whereas all 11 saplings that survived remained below this threshold (e.g. Fig. 8a), indicating a very steep transition between zero probability and complete probability of death at $PLC_p \approx 84.9$ ($P < 0.001$; Fig. 8b). If maximum PLC_p was assessed at the time of desiccation (as opposed to the end-of-season projection), the threshold was lowered to $PLC_p = 77.5$, with less support ($P = 0.013$; Fig. 8b). The corresponding thresholds for PLC_x (excluding rhizosphere) were $PLC_x = 61.3$ for end-of-season projections ($P < 0.001$), and $PLC_x = 53.2$ ($P = 0.01$) at the time of desiccation (Fig. S5). Threshold results were comparable when analyzed using absolute hydraulic conductance instead of PLC (Fig. S6).

Saplings that died tended to develop more negative P_{pd} earlier in the season than saplings that survived, and hence dying saplings had shallower estimated rooting depths on average (0.34 m, ± 0.13 SD, *n* = 5) than saplings that survived (0.94 m, ± 0.42 SD, *n* = 7).

Discussion

The gain–risk algorithm performed reasonably well at predicting xylem pressures, fluxes and conductances in response to environmental cues and known root-zone water availability (Objective I). Results were comparable to Tuzet's empirical model, but with the advantage of trait- and process-based input. There was little loss in predictive ability when adding the root-zone water budget with continuous time steps (Objective II). This result means that the model can be used to predict entire growing seasons from

initial conditions and micrometeorologic drivers. The model was capable of tracking drought responses, including hydraulic thresholds that can be used to predict the risk of mortality within a growing season.

The tendency for the gain–risk model to predict a flatter-than-measured response to environmental conditions (Fig. 5) was primarily because it under-estimated the pressure drop and consequent fluxes under wet soil moisture conditions early in the season. The pattern is best seen in the control treatment where P_{pd} was essentially constant (mean −0.38 MPa). According to the Sobol analysis, P_{pd} is the major influence on model output (Fig. 6), so control predictions were fairly constant across the growing season. The model was accurate for control K_p, which varied little (Fig. 4a). However, the model's prediction of P_{md} was only accurate for the last two-thirds of the season. In the first third, the observed P_{md} was more negative than predicted (Fig. 2a). The under-prediction of the early-season pressure drop led to the under-estimate of early-season *E* (Fig. 3e) and sapflow (Fig. 8a; also G_w). The gain–risk algorithm predicts a large pressure drop if photosynthetic capacity is high (greater gain) or the xylem vulnerability curves are resistant (low risk). Of these inputs, the most influential is VC_l (Fig. 6a), which is also the input for which we had the least temporal resolution, being measured once near the end of the season. In addition, we intentionally did not attempt to model the ambiguities of extra-xylary hydraulic conductance in the leaf. Better resolution of these inputs should improve model performance.

At the other end of the flow path from the leaf, R_{rh} was estimated to have a significant impact on K_p and hence fluxes as soil dried. The 50% estimate is the *average* over P_s from 0 to P_{crit}: as
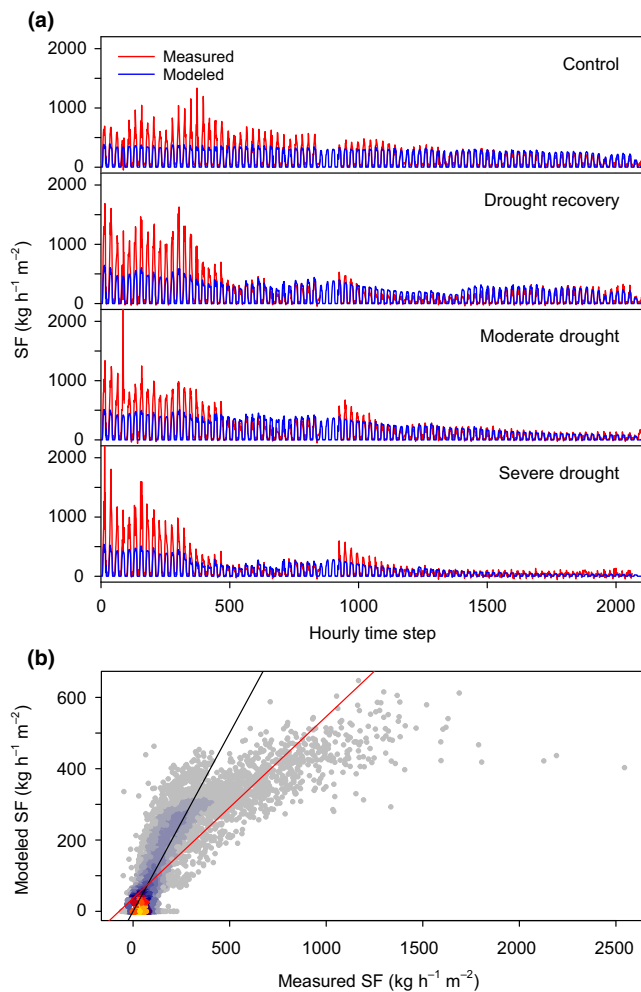
Fig. 7 Comparison between modeled and measured aspen sap flow (SF). (a) Hourly time course of the mean SF of the core trees of each treatment (red lines, measured; blue lines, modeled). (b) Modeled vs measured mean treatment SF for hourly time steps during the growing season. Colors indicate the density of points from highest density (yellow) to lowest (blue to grey). Black line represents the 1 : 1 relationship, and the red line the least square means linear regression.

the soil dries the actual percentage rises from zero to a maximum at intermediate P_s, before falling again as xylem cavitation accumulates (Sperry *et al.*, 2017). Corroborating evidence for a significant R_{rh} in drying soil was the observation that per cent soil-canopy resistance in the leaf fell by almost half from 86% under well-watered conditions to 44% in droughted plants. This trend was predicted by the model, and can only be the result of rising resistance outside of the leaves. The resistance is more than can be accounted for by cavitation in stems and roots, hence indicating a significant rhizosphere contribution. Similarly high average R_{rh} has been estimated before (Wolfe *et al.*, 2016), which suggests it may be an essential element for hydraulic models. The presence of a large rhizosphere component complicates the interpretation of hydraulic recovery in that the rhizosphere portion of K_p may be more reversible than the xylem portion (Figs 4, 8).

The uncertainty of the xylem refilling setting had little impact on the model fit in the present case. This was because observed

K_p showed an intermediate degree of recovery that was bracketed by the model's refilling vs no-refilling output (Fig. 4). In addition, even in no-refilling mode the model predicted some K_p rebound from rhizosphere recovery. The observed recovery in K_p included a rapid and limited rise seen after the major rain event on day 207 (Fig. 4); this was consistent with a reversible rhizosphere component. However, there was also a delayed but substantial increase in K_p during the rewatering phase of the drought-recovery treatment (Fig. 4b) that was probably the result of recovery in the xylem pathway. New vessel growth was probably not responsible because we did not observe a significant increase in basal area of these saplings. Vessel refilling under well-watered conditions has been observed in aspen, causing a similarly gradual recovery during the growing season (Love & Sperry, 2018). A better understanding of post-drought xylem hydraulics should improve model performance.

It is important that the model could mechanistically couple the root-zone water budget with plant pressures and fluxes. Accuracy was improved by adjusting the field capacity downward to match control P_{pd}. The lower field capacity would be consistent with an underestimation of the soil rock fraction, which only measured rocks larger than *c.* 1.2 cm in diameter. The field capacity adjustment may also have compensated for predawn disequilibrium if there was night-time transpiration or growth-induced uptake. Rooting depth was also tuned, but the estimates were realistic for aspen (mean of 0.67 m; Gifford, 1966), particularly after a year of well-watered establishment growth. The estimates also predicted the intuitive pattern that saplings dying from drought had shallower root systems than those that survived. Once these two calibrations were made, the model's success in solving the P_{pd} time series over a wide range of drought and rewatering treatments gave confidence in the van Genuchten functions and the calculation of the numerous water fluxes involved.

The linkage observed between projected loss of soil-plant hydraulic conductance and sapling desiccation and death (Fig. 8) adds to the evidence that hydraulic thresholds can predict risk of drought mortality (Anderegg *et al.*, 2015; Adams *et al.*, 2017; Tai *et al.*, 2017). Thresholds do not represent complete hydraulic failure (i.e. 100 PLC), because limited hydraulic capacity remains. In our case, the *projected* full-season maximum PLC_p was a better predictor of mortality than the maximum PLC_p at canopy desiccation. In other words, regardless of when individual trees desiccated, they all had a common trajectory of severe PLC_p by season's end. The basis for this result is unknown, but an increase in the rate of decline in P_{pd} could be a trigger. The consequence for the model is that it cannot predict the day of desiccation or death as confidently as the relative risk among trees, i.e. which are likely to die and which are likely to survive. The exact mortality threshold in PLC may depend on the species (e.g. Davis *et al.*, 2002; Rice *et al.*, 2004; Brodribb & Cochard, 2009; McDowell *et al.*, 2013) and where the hydraulic conductance was assessed. Our 85 PLC threshold was for the soil-canopy flow path, which corresponded to 61 PLC for the xylem only (no rhizosphere). These values are within the range of previously reported thresholds for aspen and other angiosperms (Anderegg *et al.*, 2015; Adams *et al.*, 2017; Tai *et al.*, 2017).

Fig. 8 Relationship between aspen mortality and whole-plant per cent loss in hydraulic conductance (PLC$_p$). (a) Modeled PLC$_p$ time course of four saplings (no xylem refilling). Solid black lines are for live saplings, and solid red lines are projected beyond death. Recovery seen in PLC$_p$ is in the rhizosphere and not the xylem. Red circle indicates the projected maximum full-season PLC$_p$ for dead saplings. Magenta triangle is the maximum PLC$_p$ reached before death. Black circle and white triangle represents the maximum seasonal PLC$_p$ reached in surviving trees. Thresholds assessed in (b) are shown as horizontal lines. Red dashed line is the threshold PLC$_p$ assessed over the full season. Magenta dash-dot line is the threshold assessed at time of death. (b) Thresholds of mortality risk vs maximum PLC$_p$ determined from logistic regression (solid lines). Black circles around white triangles at zero probability are surviving aspen. Magenta triangles at death probability = 1 are dead trees with PLC$_p$ assessed at death, and magenta line is logistic regression ($P < 0.012$), with a threshold at the magenta diamond. Red circles are dead trees with PLC$_p$ assessed over the full season, and the red line and diamond the corresponding logistic model ($P < 0.001$) and threshold.
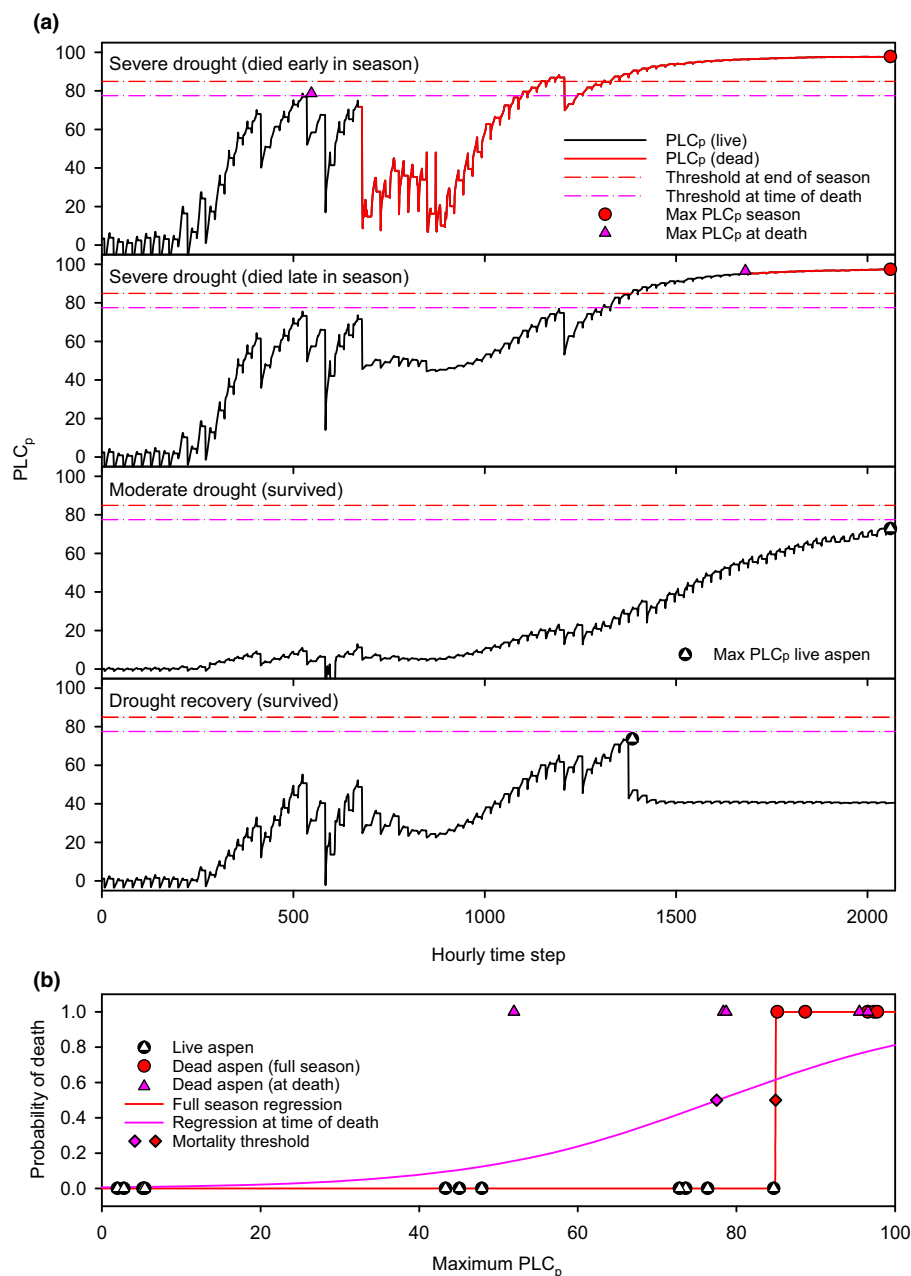
The gain–risk model is qualitatively different from empirical models of similar scale, in that it is process-based and its inputs are physical traits that are at least potentially measurable (Fig. 1; Table 1). For our purpose of testing the algorithm we minimized parameter error by 'tuning' three traits: two were difficult to measure directly (R_{rh} and rooting depth) and the third (field capacity) was calibrated for internal consistency with control predawn xylem pressure. Results were comparable to Tuzet's empirical model where its three coefficients were similarly tuned. The advantage of the gain–risk model comes when it is being applied to make true forecasts vs being tested with hindcasting as in the present case. All parameters of the gain–risk model are identifiable traits whose values and uncertainties can be specified. These traits dictate the short-term drought response, and known uncertainty in trait values can be readily propagated to uncertainty in

the prediction. By contrast, the value and uncertainty of Tuzet coefficients (and those of similar models) cannot be so easily set because c_1, c_2 and P_{ref} are not specific, identifiable photosynthetic or hydraulic properties. Their values are dictated by the drought response, and unknowable *a priori*. A trait-based approach should also facilitate the incorporation of feedbacks between short-term responses and longer-term trait adjustments, as would be necessary for predicting beyond a single growing season.

Acknowledgements

Author contributions

M.D.V., J.S.S., D.M.L., Y.W. and W.R.L.A. designed the experiment. M.D.V., D.M.L. and Y.W. established the research garden. M.D.V., D.M.L., E.H.F. and M.G.A. performed the measurements. J.S.S. coded the model. M.D.V., J.S.S. and D.M.L. analyzed the data. M.D.V. and J.S.S. led the writing. All authors contributed to data interpretation, discussion and the final version.

ORCID

Martin D. Venturas (iD) http://orcid.org/0000-0001-5972-9064
David M. Love (iD) http://orcid.org/0000-0002-0582-6990
Yujie Wang (iD) http://orcid.org/0000-0002-3729-2743

References

Adams HD, Zeppel MJ, Anderegg WR, Hartmann H, Landhäusser SM, Tissue DT, Huxman TE, Hudson PJ, Franz TE, Allen CD et al. 2017. A multi-species synthesis of physiological mechanisms in drought-induced tree mortality. *Nature Ecology & Evolution* 1: 1285.

Alder NN, Pockman WT, Sperry JS, Nuismer S. 1997. Use of centrifugal force in the study of xylem cavitation. *Journal of Experimental Botany* 48: 665–674.

Allen C, Macalady A, Chenchouni H, Bachelet D, McDowell N, Vennetier M, Kitzberger T, Rigling A, Breshears D, Hogg EH et al. 2010. A global overview of drought and heat-induced tree mortality reveals emerging climate change risks for forests. *Forest Ecology and Management* 259: 660–684.

Anderegg WRL, Berry JA, Smith DD, Sperry JS, Anderegg LDL, Field CB. 2012. The roles of hydraulic and carbon stress in a widespread climate-induced forest die-off. *Proceedings of the National Academy of Sciences, USA* 109: 233–237.

Anderegg WRL, Flint A, Huang C, Flint L, Berry JA, Davis F, Sperry JS, Field CB. 2015. Tree mortality predicted from drought-induced vascular damage. *Nature Geoscience* 8: 367–371.

Anderegg WR, Wolf A, Arango-Velez A, Choat B, Chmura DJ, Jansen S, Kolb T, Li S, Meinzer F, Pita P. 2017. Plant water potential improves prediction of empirical stomatal models. *PLoS ONE* 12: e0185481.

Anderegg WR, Wolf A, Arango-Velez A, Choat B, Chmura DJ, Jansen S, Kolb T, Li S, Meinzer FC, Pita P et al. 2018. Woody plants optimise stomatal behaviour relative to hydraulic risk. *Ecology Letters* 21: 968–977. doi: 10.1111/ele.12962.

Baker J, van Bavel C. 1987. Measurement of mass flow of water in the stems of herbaceous plants. *Plant, Cell & Environment* 10: 777–782.

Brodribb T, Bowman DJ, Nichols S, Delzon S, Burlett R. 2010. Xylem function and growth rate interact to determine recovery rates after exposure to extreme water deficit. *New Phytologist* 188: 533–542.

Brodribb TJ, Cochard H. 2009. Hydraulic failure defines the recovery and point of death in water-stressed conifers. *Plant Physiology* 149: 575–584.

Brodribb T, Holbrook N, Edwards E, Gutierrez M. 2003. Relations between stomatal closure, leaf turgor and xylem vulnerability in eight tropical dry forest trees. *Plant, Cell & Environment* 26: 443–450.

Buckley TN, Mott KA. 2013. Modelling stomatal conductance in response to environmental factors. *Plant, Cell & Environment* 36: 1691–1699.

Campbell GS. 1985. *Soil physics with BASIC: transport models for soil-plant systems.* Amsterdam, the Netherlands: Elsevier.

Campbell GS, Norman JN. 1998. *An introduction to environmental biophysics.* New York, NY, USA: Springer.

Collatz GJ, Ball JT, Grivet C, Berry JA. 1991. Physiological and environmental regulation of stomatal conductance, photosynthesis and transpiration: a model that includes a laminar boundary layer. *Agricultural and Forest Meteorology* 54: 107–136.

Davis SD, Ewers FW, Portwood KA, Sperry JS, Crocker MC, Adams GC. 2002. Shoot dieback during prolonged drought in *Ceanothus* chaparral in California: a possible case of hydraulic failure. *American Journal of Botany* 89: 820–828.

Drake J, Power S, Duursma R, Medlyn B, Aspinwall M, Choat B, Creek D, Eamus D, Maier C, Pfautsch S. 2017. Stomatal and non-stomatal limitations of photosynthesis for four tree species under drought: a comparison of model formulations. *Agricultural and Forest Meteorology* 247: 454–466.

Fisher RA, Koven CD, Anderegg WR, Christoffersen BO, Dietze MC, Farrior CE, Holm JA, Hurtt GC, Knox RG, Lawrence PJ et al. 2018. Vegetation demographics in Earth System Models: a review of progress and priorities. *Global Change Biology* 24: 35–54.

Frazer G, Canham C, Lertzman K. 1999. Gap Light Analyzer (GLA): imaging software to extract canopy structure and gap light transmission indices from true-colour fisheye photographs. Users manual and program documentation, Version 2.0. Simon Fraser University, Burnaby, British Columbia, and the Institute of Ecosystem Studies, Millbrook, New York, USA.

Gifford GF. 1966. Aspen root studies on three sites in northern Utah. *American Midland Naturalist* 75: 132–141.

IPCC. 2014. Climate Change 2014: Synthesis Report. *Contribution of Working Groups I, II and III to the Fifth Assessment Report of the Intergovernmental Panel on Climate Change* [Core Writing Team, R. K. Pachauri, L. A. Meyer (eds.)]. IPCC, Geneva, Switzerland.

Jones HG, Sutherland R. 1991. Stomatal control of xylem embolism. *Plant, Cell & Environment* 14: 607–612.

Kolb KJ, Sperry JS, Lamont BB. 1996. A method for measuring xylem hydraulic conductance and embolism in entire root and shoot systems. *Journal of Experimental Botany* 47: 1805–1810.

Love DM, Sperry JS. 2018. In situ embolism induction reveals vessel refilling in a natural aspen stand. *Tree Physiology* 38: 1006–1015.

McDowell N, Fisher RA, Xu C, Domec JC, Holtta T, Mackay DS, Sperry JS, Boutz A, Diskman L, Geheres N et al. 2013. Evaluating theories of drought-induced vegetation mortality using a multimodel-experimental framework. *New Phytologist* 200: 304–321.

Medlyn BE, Dreyer E, Ellsworth DS, Forstreuter M, Harley PC, Kirschbaum MUF, LeRoux X, Montpied P, Strassemeyer J, Walcroft A et al. 2002. Temperature response of parameters of a biochemically based model of photosynthesis. II. A review of experimental data. *Plant, Cell & Environment* 25: 1167–1179.

Menard SW. 2002. *Applied logistic regression analysis.* London, UK: Sage Publications.

Nossent J, Elsen P, Bauwens W. 2011. Sobol'sensitivity analysis of a complex environmental model. *Environmental Modelling & Software* 26: 1515–1525.

Powell T, Galbraith D, Christoffersen B, Harper A, Imbuzeiro H, Rowland L, Almeida S, Brandom P, da Costa A, MaLN Costa et al. 2013. Confronting model predictions of carbon fluxes with measurements of Amazon forests subjected to experimental drought. *New Phytologist* 200: 350–365.

Resco V, Ewers BE, Sun W, Huxman TE, Weltzin J, Williams DG. 2009. Drought-induced hydraulic limitations constrain leaf gas exchange recovery after precipitation pulses in the C3 woody legume, *Prosopis velutina. New Phytologist* 181: 672–682.

Rice KJ, Matzner SL, Byer W, Brown JR. 2004. Patterns of tree dieback in Queensland, Australia: the importance of drought stress and the role of resistance to cavitation. *Oecologia* 139: 190–198.

Rodríguez-Calcerrada J, Li M, López R, Cano FJ, Oleksyn J, Atkin OK, Pita P, Aranda I, Gil L. 2017. Drought-induced shoot dieback starts with massive root

xylem embolism and variable depletion of nonstructural carbohydrates in seedlings of two tree species. *New Phytologist* 213: 597–610.

Sakuratani T. 1981. A heat balance method for measuring water flux in the stem of intact plants. *Journal of Agricultural Meteorology* 37: 9–17.

Smith NG, Rodgers VL, Brzostek ER, Kulmatiski A, Avolio ML, Hoover DL, Koerner SE, Grant K, Jentsch A, Fatichi S. 2014. Toward a better integration of biological data from precipitation manipulation experiments into Earth system models. *Reviews of Geophysics* 52: 412–434.

Sperry JS, Love DM. 2015. What plant hydraulics can tell us about plant responses to climate-change droughts. *New Phytologist* 207: 14–27.

Sperry JS, Venturas MD, Anderegg WR, Mencuccini M, Mackay DS, Wang Y, Love DM. 2017. Predicting stomatal responses to the environment from the optimization of photosynthetic gain and hydraulic cost. *Plant, Cell & Environment* 40: 816–830.

Sperry JS, Wang Y, Wolfe B, Mackay DS, Anderegg WRL, McDowell NG, Pockman WT. 2016. Pragmatic hydraulic theory predicts stomatal responses to climatic water deficits. *New Phytologist* 212: 577–589.

Tai X, Mackay DS, Anderegg WR, Sperry JS, Brooks PD. 2017. Plant hydraulics improves and topography mediates prediction of aspen mortality in southwestern USA. *New Phytologist* 213: 113–127.

Tukey JW. 1977. *Exploratory data analysis*. Boston, MA, USA: Addison-Wesley Publishing Co.

Tuzet A, Perrier A, Leuning R. 2003. A coupled model of stomatal conductance, photosynthesis and transpiration. *Plant, Cell & Environment* 26: 1097–1116.

Tyree MT, Sperry JS. 1988. Do woody plants operate near the point of catastrophic xylem dysfunction caused by dynamic water stress? Answers from a model. *Plant Physiology* 88: 574–580.

Venturas MD, MacKinnon ED, Dario HL, Jacobsen AL, Pratt RB, Davis SD. 2016. Chaparral shrub hydraulic traits, size, and life history types relate to species mortality during California's historic drought of 2014. *PLoS ONE* 11: e0159145.

Venturas MD, Sperry JS, Hacke UG. 2017. Plant xylem hydraulics: what we understand, current research, and future challenges. *Journal of Integrative Plant Biology* 59: 356–389.

Wolf A, Anderegg WRL, Pacala SW. 2016. Optimal stomatal behavior with competition for water and risk of hydraulic impairment. *Proceedings of the National Academy of Sciences, USA* 113: E7222–E7230.

Wolfe B, Sperry JS, Kursar T. 2016. Does leaf shedding protect stems from cavitation during seasonal droughts? A test of the hydraulic fuse hypothesis. *New Phytologist* 212: 1007–1018.

Supporting Information

Additional Supporting Information may be found online in the Supporting Information section at the end of the article.

Fig. S1 Experimental design of the research plot.

Fig. S2 Midday weather input variables for the days in which we compare measured vs modeled output variables running the model from predawn pressures (Objective I).

Fig. S3 Hourly measurements of the main weather inputs required for running the water budget model (Objective II).

Fig. S4 Studentized measured vs Tuzet model output treatment means.

Fig. S5 Water budget model drought mortality predictive capacity based on whole-plant xylem per cent loss in hydraulic conductance.

Fig. S6 Water budget model drought mortality predictive capacity based on whole-plant conductance and xylem conductance.

Table S1 Excel file containing the main dataset of this study

Methods S1 Modeling canopy sun and shade layers, and evaporation from soil.

Methods S2 Tuzet model fitting.

Methods S3 Measurement of rock volume in the soil.

Methods S4 Construction of A–Ci curves.

Notes S1 Model code comments

Notes S2 Excel file with Visual Basic Application macro for setting saturated values for K (K_{max}) and percentage of resistance in the leaf.

Notes S3 Excel file containing the Visual Basic Application macro for the model run from predawn xylem pressures.

Notes S4 Excel file containing the Visual Basic Application macro for running Tuzet's model from predawn xylem pressures.

Notes S5 Excel file containing the Visual Basic Application macro for the full water budget model.

Please note: Wiley Blackwell are not responsible for the content or functionality of any Supporting Information supplied by the authors. Any queries (other than missing material) should be directed to the *New Phytologist* Central Office.